Published in: ***Proceedings of the 7th. Int. Conf. on Thermal, Mechanical and Multiphysics Simulation and Experiments in Micro-Electronics and Micro-Systems, EuroSimE 2006, Como, Italy***
Status: Postprint (Author's version)
DOI: 10.1109/ESIME.2006.1643959

Finite Element Modeling of Electrostatic MEMS Including the Impact of Fringing Field Effects on Forces

M. Boutaayamou, K. H. Nair, R. V. Sabariego, P. Dular
Dept. of Electrical Engineering and Computer Science (ELAP)
University of Liege, Sart Tilman Campus, Building B28, B-4000, Liege, Belgium
Contact: mboutaayamou@ulg.ac.be, +32 (0) 4 366 37 10

Abstract

The numerical models describing the behaviour of electrostatically actuated microsystems often disregard fringing fields. However, taking the fringing fields into account is crucial for an accurate computation of the electrostatic forces. In this work, the finite element method is applied for modeling electrostatic actuators. The electrostatic force distribution is obtained by locally applying the virtual work method. A micro-beam and a comb drive are considered as test cases. The impact of the fringing field effects on the accuracy of electrostatic forces is shown through 2D and 3D parametric studies.

1. Introduction

Microelectromechanical systems (MEMS) are integrated micro devices or systems consisting of electrical and mechanical components. These systems are widely used as sensors and actuators on the micro scale. Electrostatic actuation is predominantly opted for most microactuators due to its good mechanical flexibility, high energy density and low power consumption.

Structurally, a simple electrostatically actuated microsystem consists of an upper cantilever beam (movable) and a lower ground electrode (fixed). In such a system, the deflection caused by differences of potential and the redistribution of charges due to the change in geometry constitute the strong coupling between the mechanical and electrostatic models [1]. Several mathematical models have been developed to compute the electrostatic forces [2], [3]. These are however often established on a mass-spring model under geometric and electrostatic assumptions [4] that usually neglects the fringing fields.

The finite element (FE) method is here applied for modeling microelectromechanical devices considering the fringing field effects. Through 2D and 3D analyses, the aim is to demonstrate the impact of the fringing effects on the evaluation of the electrostatic forces. The local electrostatic forces are computed by means of the virtual work method [5].

A micro-beam and a comb drive are considered as test cases. Results of 2D and 3D geometrical parametric studies are discussed and the influence of fringing field effects is evidenced.

2. Finite Element Formulations of MEMS

An electrostatic problem is considered in a domain Ω. It consists of computing the electric field **e** in Ω, and ensuing quantities such as the electric forces, the sources of which are conductors with applied voltages.

The electric field **e** derives from an electric scalar potential v, i.e. **e** = – **grad** v. The electric potential can be set to a constant value on each conductor to account for the voltage sources. The electrostatic problem can be solved via the weak form of the Poisson equation, div ($-\varepsilon$ **grad** v) = q, i.e.,

$$(-\varepsilon\,\mathbf{grad}\,v\,,\mathbf{grad}\,v')_{\Omega} + (q,v')_{\Omega} - <\mathbf{n}\cdot\mathbf{d},v'>_{\Gamma_d} = 0,\ \forall\, v' \in F(\Omega), \tag{1}$$

where ε is the electric permittivity, q is the electric charge density, **d** is the electric flux density (with **d** = ε **e**) and $F(\Omega)$ is the function space defined on Ω containing the basis functions for v as well as for the test function v' [6]; $(\cdot\,,\cdot\,)_{\Omega}$ and $<\cdot\,,\cdot>_{\Gamma}$ respectively denote a volume integral in Ω and a surface integral on Γ of products of scalar or vector fields. The surface integral term in (1) is used for fixing a natural boundary condition (usually homogeneous for a tangent electric field constraint) on a portion Γ_d of the boundary of Ω; the normal **n** is exterior to Ω.

In charge free regions, (1) reduces to

$$(-\varepsilon\,\mathbf{grad}\,v\,,\mathbf{grad}\,v')_{\Omega} - <\mathbf{n}\cdot\mathbf{d},v'>_{\Gamma_d} = 0,\ \forall\, v' \in F(\Omega). \tag{2}$$

The electric force distribution is calculated by locally applying the virtual work principle [5]. At the discrete level, the force at each node is obtained by deriving the electric energy in the surrounding elements with respect to the displacement. Let us assume that the movable part of a rigid body is surrounded by free space, the contribution of a reference element Δ to the force in a given direction is

Published in: ***Proceedings of the 7th. Int. Conf. on Thermal, Mechanical and Multiphysics Simulation and Experiments in Micro-Electronics and Micro-Systems, EuroSimE 2006, Como, Italy***
Status: Postprint (Author's version)
DOI: 10.1109/ESIME.2006.1643959

$$F_u = \int_\Delta \frac{\varepsilon}{2}\left(-2\mathbf{e}J^{-1}\frac{\partial J}{\partial u}\mathbf{e}|J| + \mathbf{e}\mathbf{e}\frac{\partial |J|}{\partial u}\right) d\Delta, \tag{3}$$

for a virtual displacement u in this direction. J is the geometrical Jacobian matrix and $|J|$ is its determinant.

The derivative in (3) has to be performed by keeping the electric field **e** constant, which is ensured by the nodal element discretisation [7].

3. Application Examples

Two electrostatically actuated MEM devices, namely a micro-beam and a comb drive, are modeled using the FE method. The electric forces are computed by means of the virtual work method. The aim is to explore via 2D and 3D analyses the strong dependence of fringing field effects on geometrical parameters when these structures are subjected to voltages.

Micro-beam

A micro-beam is studied as first test case (Fig. 1). The considered geometrical parameters are the air gap g (distance between both electrodes), the length L, the width w and the thickness t of the beam. These parameters are varied in order to determine the effect of the fringing fields in the accurate computation of the force. The applied voltage is fixed to 5V.

A factor, hereafter called the fringing factor, is defined as the relative difference between the electrostatic force F^f computed by the virtual work method on the actual geometry with the finite element method and the force estimated analytically F^{nf} by neglecting the fringing fields, i.e.

$$\text{Fringing factor} = \frac{F^f - F^{nf}}{F^{nf}}. \tag{4}$$

The analytical expression for the transverse force acting on the beam without any fringing correction is given by

$$F^{nf} = \frac{1}{2}\varepsilon_0 S \frac{V^2}{g^2}, \tag{5}$$

where S is the surface area of the beam section facing the ground electrode and V is the applied voltage.

Both 2D and 3D models are considered. The 3D model considers both the finite length and width of the beam. A first 2D model is defined for the transverse cross section of the beam, thus neglecting the finite length fringing effects. The reference beam length L is fixed to 30 µm. The fringing factor is shown in Figs. 2 and 3 for different values of the ratios w/g and w/t, respectively.

As expected, the fringing factor is always higher in the 3D cases, these considering the fringing fields at the beam end. Moreover, for a constant L, the fringing factor increases with a decrease of the ratios w/g and w/t, i.e. the effects of fringing fields dominate when increasing either g or t for a fixed value of w, or when the width w decreases for fixed values of g and t.

A second 2D model considers then the longitudinal cross section of the beam. This time, it thus neglects the finite width fringing effects. Figs. 4 and 5 represent the fringing factor for different values of the ratios L/g and L/t respectively. The fringing increases when these ratios diminish, i.e. when the values of g and t increase for a fixed value of L, or when the length L decreases for fixed values of g and t.

In order to point out the influence of the mesh refinement on the computation accuracy of the electrostatic force, different discretisations of the beam microsystem are considered. The geometrical parameters are defined as: L = 30 µm, w = 2 µm, t = 1 µm and g = 1 µm.

A dimension l_c is defined as the average size of the finite elements in the neighborhood of the corners of the beam. The relative error is computed taking the finest mesh as reference for both 2D and 3D cases. Fig. 6 illustrates the obtained relationship between the relative error and the average size l_c of the finite elements in the neighborhood of the corners. It can be seen that the relative error can be reduced to a few percents with a element size lower than about the tenth of the lowest characteristic dimensions of the beam.

Comb drive

A comb drive is considered as a second test case. It consists of two combs typically arranged so that they can slide past one another until each finger occupies the slot in the opposite comb. The modeling of such a structure can be reduced to the half of two opposite fingers taking advantage of the periodicity conditions. The electric field is tangent to both cut surfaces Γ_d, i.e. $\mathbf{n} \cdot \mathbf{d} = 0$ on Γ_d is used in (1). Fig. 7 shows the considered geometry of the microsystem with the length of the finger L, its width b, its thickness t, the gap between fingers g and the length of the overlap L-d.

Published in: ***Proceedings of the 7th. Int. Conf. on Thermal, Mechanical and Multiphysics Simulation and Experiments in Micro-Electronics and Micro-Systems, EuroSimE 2006, Como, Italy***
Status: Postprint (Author's version)
DOI: 10.1109/ESIME.2006.1643959

Figs. 8 and 9 show examples of finite element meshes used for solving the electrostatic field problem in 2D and 3D cases respectively**.** Note that in both cases, the air region adjacent to the tip of the comb finger is finely meshed to reduce the error on the fringing field.

Fig. 10 shows the distribution of the electric force density on the fingers boundaries. It points out the increase of the force density at the corners.

The analytical expressions for estimating the electric forces along *x* and *y* axes, i.e. in longitudinal and transversal directions, are respectively [8]

$$F_x^{nf} = \frac{1}{2}\varepsilon_0 \frac{ntV^2}{g} + \frac{1}{2}\varepsilon_0 \frac{btV^2}{d^2}, \tag{7}$$

$$F_y^{nf} = \frac{1}{2}\varepsilon_0 S \frac{V^2}{g^2}, \tag{8}$$

where n is the number of the pairs of electrodes (here $n = 2$), V is the applied voltage and S is the surface area of the section of the overlapping finger given by $(L - d)\,t$. Particularizing (4) with (7) and (8), we obtain the corresponding fringing factor along *x* and *y* axes.

Fig. 11 shows that the fringing factor for the longitudinal force becomes significant for some ratios *b/t* of the fingers for both 2D and 3D cases. The important difference between the curves representing fringing factor in 2D and 3D cases is due to the influence of the thickness *t* for a fixed value of the width. Fig. 12 shows that, for a fixed thickness *t*, the fringing factor of the transversal force (along the *y*-axis) decreases as the overlap length $(L - d)$ between the two fingers increases. These behaviors are in accordance with those pointed out for the beam model.

Conclusion

The presence of fringing fields in two-dimensional and three-dimensional models of electrostatic micro devices, such as a micro-beam and a comb drive, has been emphasized and their effect on the accuracy of electrostatic forces has been represented via a fringing factor. The impact of the fringing fields with varying dimensions of microstructures has been pointed out through parametric studies and reveals the necessity to make use of 3D models for their accurate evaluation.

The calculated electrostatic forces increase considerably due to the fringing field effects. The accurate calculation of these forces is crucial for an accurate evaluation of the mechanical displacements in electrostatically actuated microstructures.

Acknowledgements

This work is supported by the Belgian Science Policy (IAP P5/34) and the Belgian French Community (ARC 03/08-298). P. Dular is a Research Associate with the Belgian National Fund for Scientific Research (F.N.R.S.).

References

1. Schwarzenbach H.U. et al, "A microelectro mechanical CAD extension for SESES," *Journal of Micromechanics and Microengineering*, No. 3 (1993), pp. 118–122.
2. Artz B.E. and Cathey L.W., "A Finite Element Method for Determining Structural Displacements Resulting from Electrostatic Forces," *Proc. IEEE Solid State Sensor and Actuator Workshop*, Hilton Head, SC, June. 1992, pp. 190–193.
3. Raback P. and Pursula A, "Finite Element Simulation of The Electro-Mechanical Pull-In Phenomenon," *ECCOMAS* 2004, Jyväskylä, July. 2004, pp. 24–28.
4. Osterberg, P.M. and Senturia, S.D., "M-TEST: A Test Chip for MEMS Material Property Measurement Using Electrostatically Actuated Test Structures," *Journal of Microelectromechanical Systems*, Vol. 6, No. 2 (1997), pp. 107–118.
5. Coulomb J.L., Meunier G., "Finite Element Implementation of Virtual Work Principle for Magnetic or Electric Force and Torque Computation," *IEEE Transactions on Magnetics*, Vol. 20, No. 5 (1984), pp. 1894–1896.
6. P. Dular, W. Legros, A. Nicolet, "Coupling of Local and Global Quantities in Various Finite Element Formulations and its Application to Electrostatics, Magnetostatics and Magnetodynamics," *IEEE Transactions on Magnetics*, Vol. 34, No. 5 (1998), pp. 3078–3081.
7. Gérard Meunier, Modèles et formulations en électromagnetisme – electromagnétisme et éléments finis 2, Lavoisier (Paris, 2002), pp. 21–88.
8. Hirano T., Furuhata T., Gabriel K.J. and Fujita H., "Design, fabrication and operation of submicron gap comb – drive microactuators," *Journal of Microelectromechanical Systems*, Vol. 1, No. 1 (1992), pp. 52–59.

Published in: ***Proceedings of the 7th. Int. Conf. on Thermal, Mechanical and Multiphysics Simulation and Experiments in Micro-Electronics and Micro-Systems, EuroSimE 2006, Como, Italy***
Status: Postprint (Author's version)
DOI: 10.1109/ESIME.2006.1643959

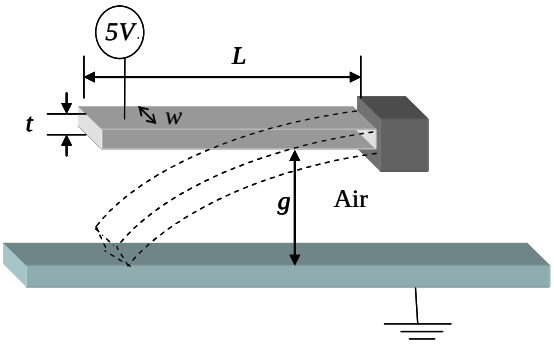

Fig. 1. Geometry of the micro-beam with length L, width w and thickness t ($\varepsilon_0 = 8.854\ 10^{-12}$ F/m).

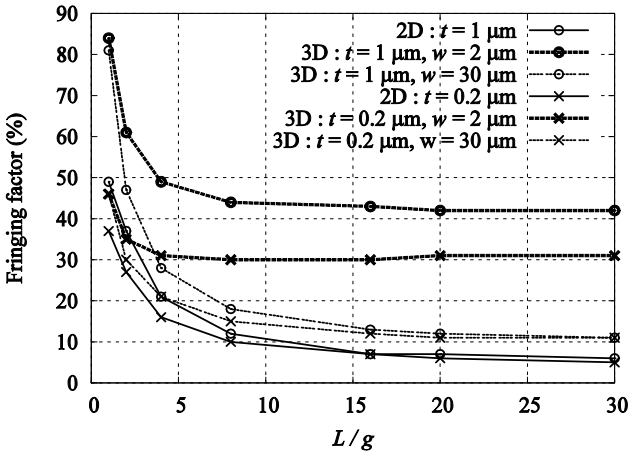

Fig. 4. Fringing factor vs L/g, showing the relative effect of the length L with respect to the gap g.

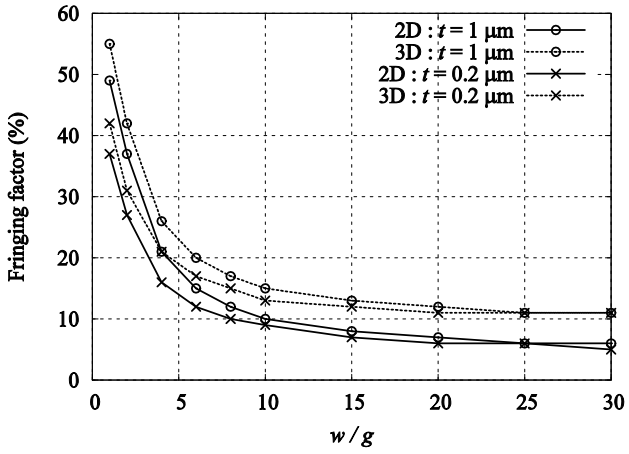

Fig. 2. Fringing factor vs w/g (L =30 µm), showing the relative effect of the width w with respect to the gap g.

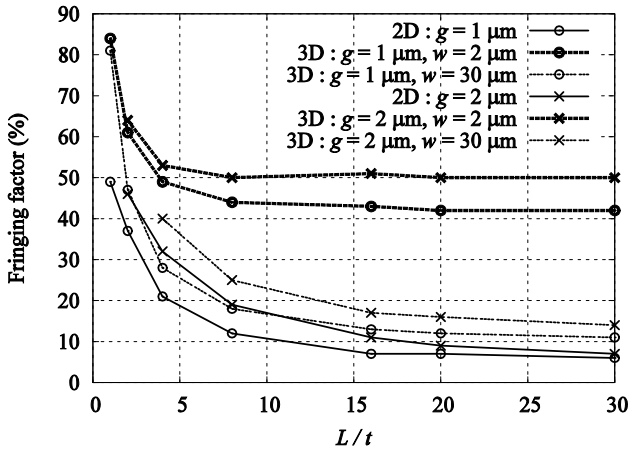

Fig. 5. Fringing factor vs L/t, showing the relative effect of the length L with respect to the thickness t.

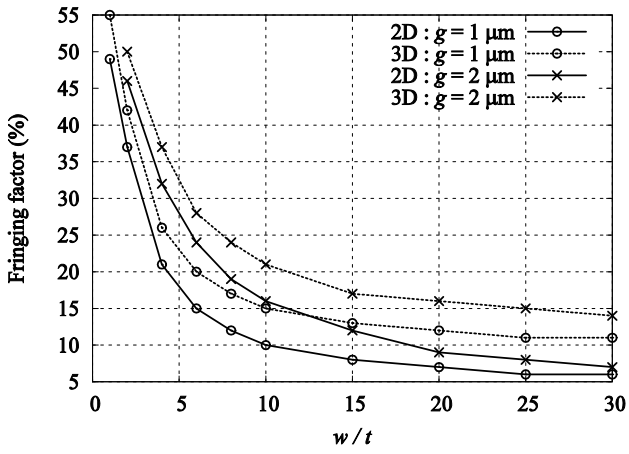

Fig. 3. Fringing factor vs w/t (L =30 µm), showing the relative effect of the width w with respect to the thickness t.

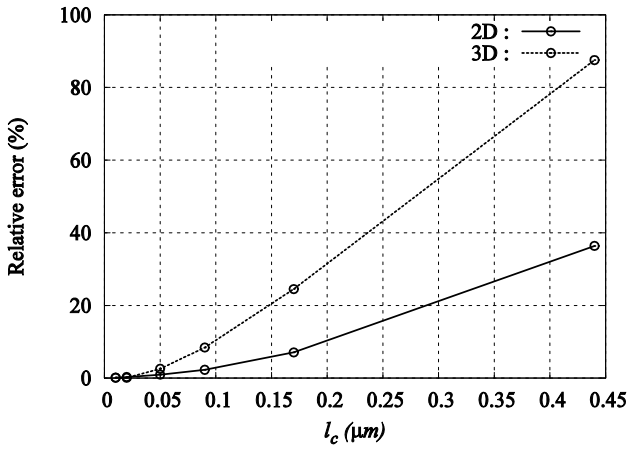

Fig. 6. Relative error vs the size l_c of the finite elements in the neighborhood of the corners (with L = 30 µm, w = 2 µm, t = 1 µm, g = 1 µm).

Published in: ***Proceedings of the 7th. Int. Conf. on Thermal, Mechanical and Multiphysics Simulation and Experiments in Micro-Electronics and Micro-Systems, EuroSimE 2006, Como, Italy***
Status: Postprint (Author's version)
DOI: 10.1109/ESIME.2006.1643959

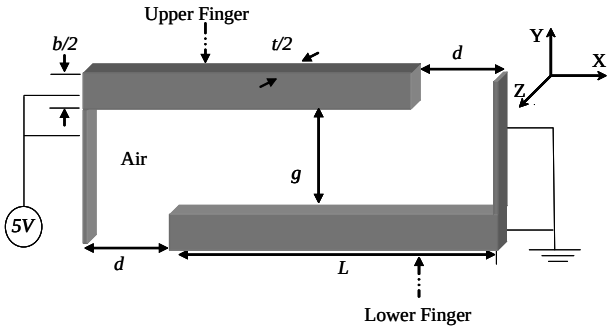

Fig. 7. Geometry of the comb-drive.

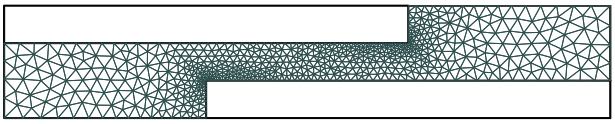

Fig. 8. 2D finite element mesh of the air region surrounding the comb fingers.

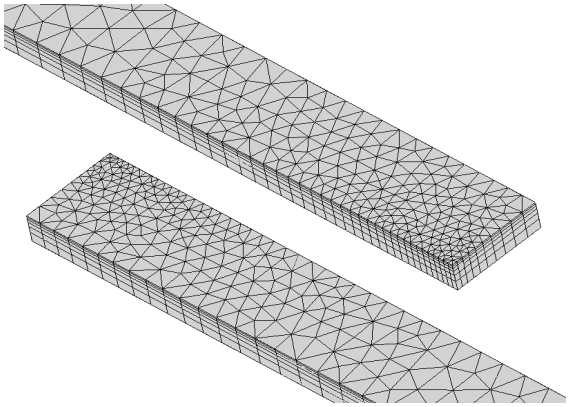

Fig. 9. Trace on the comb fingers boundaries of the surrounding 3D finite elements in the air.

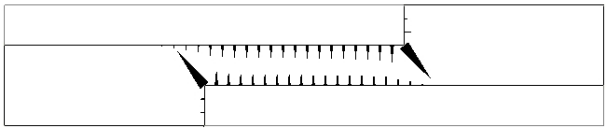

Fig. 10. Distribution of electric forces in 2D.

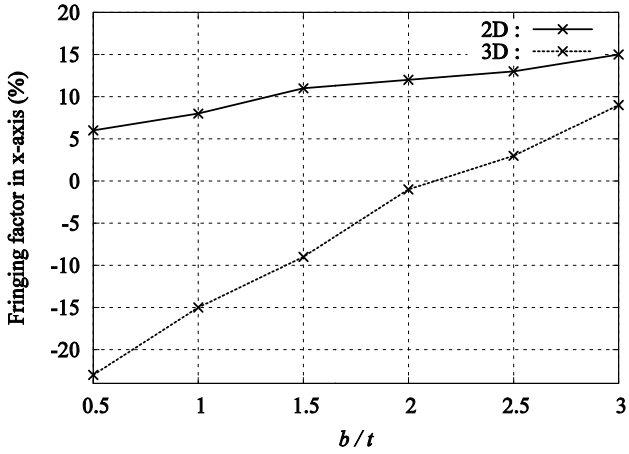

Fig. 11. Fringing factor for the longitudinal force (*x* direction) vs *b/t* (*L = 10* µm, *g = 1* µm), showing the relative effect of the width *b* with respect to the thickness *t*.

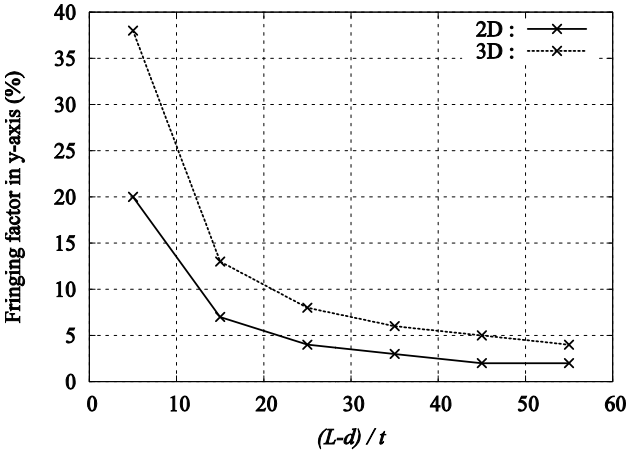

Fig. 12. Fringing factor for the transversal force (*y* direction) vs (*L-d*)/*t* (b = 2 µm, g = 1 µm), showing the relative effect of the overlap length (*L* – *d*) with respect to the thickness *t*.